The Journal of Chemical Physics

Hydrodynamic interaction facilitates the unsteady transport of two neighboring vesicles

Cite as: J. Chem. Phys. **151**, 094108 (2019); https://doi.org/10.1063/1.5113880
Submitted: 09 June 2019 . Accepted: 13 August 2019 . Published Online: 06 September 2019

Julian Lee, Sean L. Seyler, and Steve Pressé

The Journal of Chemical Physics ARTICLE scitation.org/journal/jcp

Hydrodynamic interaction facilitates the unsteady transport of two neighboring vesicles

Cite as: J. Chem. Phys. 151, 094108 (2019); doi: 10.1063/1.5113880
Submitted: 9 June 2019 • Accepted: 13 August 2019 •
Published Online: 6 September 2019

Julian Lee,[1,a] Sean L. Seyler,[2] and Steve Pressé[2,b]

AFFILIATIONS

[1] Department of Bioinformatics and Life Science, Soongsil University, Seoul 06978, South Korea
[2] Department of Physics, Arizona State University, Tempe, Arizona 85287, USA

[a] Electronic mail: jul@ssu.ac.kr
[b] Electronic mail: spresse@asu.edu

ABSTRACT

We obtain a numerical solution of the equation for the synchronous unsteady motion of two spherical vesicles in incompressible viscous fluid in the presence of both Stokes drag and hydrodynamics memory. We find that for a given amount of work performed, the final distance traveled by each vesicle is increased by the presence of the other vesicle moving in the same direction. The result suggests that the unsteady transport of the vesicles by molecular motors *in vivo* may be facilitated due to an effective hydrodynamic interaction between the neighboring vesicles.

I. INTRODUCTION

Subcellular transport processes have been the subject of continuing interest largely because of the high efficiency of molecular-scale motors responsible for such transport, as compared to the efficiency of their macroscopic counterparts.[1–13] Important factor affecting such a transport process include the hydrodynamic interactions[14–48] of the molecular motor as well as the vesicle transported by such a motor with the surrounding viscous fluid.[49] First, it has been shown that the Stokes drag experienced by a spherical object embedded in a fluid is reduced in the presence of another sphere in the vicinity.[50] The reduction of drag can be understood intuitively as coming from the indirect transfer of the momentum between the embedded objects, mediated by the fluid. Second, there is a separate effect of hydrodynamic memory due to the unsteady flow,[29–41,51–56] where the momentum transferred from an embedded object is transiently stored in the fluid and then transferred back to the object at a later point. Such an effect may facilitate the transport even for a single spherical object.[57]

These considerations motivate us to ask whether the fluid flow generated by an unsteady motion of a moving object in viscous fluid indeed facilitates the transport of a neighboring object. In fact, the equations for the unsteady motion of two hard spheres in incompressible viscous fluid have been developed recently,[40,41] but their solutions have not been provided as yet, and the implications of these equations on the efficiency of transport have not been investigated so far. To study whether the hydrodynamic interactions between neighboring spherical vesicles facilitate their unsteady transport, we consider two hard spheres under the same constant external force of finite duration. By numerically integrating the equation of motion[40,58] [Eq. (2)], we show that for a given distance traveled, the required input work for two neighboring vesicles is less than that for those separated by a larger distance. We also find that two neighboring vesicles are transported faster than separated vesicles. Our result supports the idea that indirect, fluid-induced, intervesicle interaction may be utilized in active subcellular transport for improved efficiency.

II. EQUATION FOR TWO HARD SPHERES

The equation describing an unsteady motion of two nonrotating hard spheres in incompressible viscous fluid has been derived by generalizing the equation for one sphere in a fluid.[40] Briefly, fluid flow is computed in the presence of a sphere of radius R with no-slip boundary conditions by using the unsteady Stokes equation where the advective term in the Navier-Stokes equation is neglected but the time-derivative is kept.[59] Another sphere is introduced at a center-to-center distance d, and then, the flow is perturbed in order

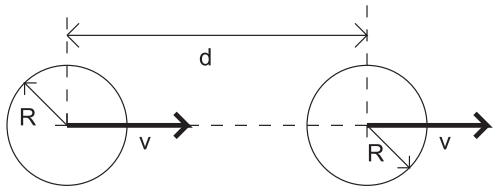

FIG. 1. The spheres moving along the center-to-center axis. The directions of the velocity are shown by the bold arrows which are also the directions of the external forces. The center-to-center distance and the radius are d and R, respectively.

to satisfy the no-slip boundary at the second sphere and perturbed again in order to satisfy the boundary condition at the first sphere. This process is iteratively repeated. The series is truncated so that the resulting error is of order ϵ^4, where $\epsilon \equiv R/d$.[40] The resulting expression for the force has a remarkable symmetry with respect to the exchange of the spheres' positions. In particular, when their radii are the same and they move with the same velocity $\mathbf{v}(t)$, the force exerted on each of the spheres is the same. In the special case of one-dimensional motion with the velocity $v(t)$ (Fig. 1) along their separation vector, the equation reduces to[40]

$$F_{\text{fluid}} = -\frac{6\pi\eta R}{1+\frac{3}{2}\epsilon-\epsilon^3}v - \frac{2\pi R^3\rho_f}{3(1+3\epsilon^3)}\dot{v} - 6\pi\eta R\int_{-\infty}^{t} dt'\dot{v}(t')h_\epsilon(t-t'), \tag{1}$$

where ρ_f and η are the density and the dynamic viscosity of the fluid, respectively. The functional form of the memory kernel $h_\epsilon(t)$ is formally given as a Laplace transform[40] (Appendix A). A similar expression can be obtained for the spheres whose motion is in the direction perpendicular to the lines joining their centers (Appendix B). Because the force exerted on each sphere by the fluid is the same, the motion of both spheres can be kept synchronous by applying the same external force $F(t)$ using the same initial velocities. The equation of motion for each sphere can be written as

$$\left(\rho_s + \frac{\rho_f}{2(1+3\epsilon^3)}\right)\dot{v} = -\frac{9\eta}{2R^2}\frac{v}{1+\frac{3}{2}\epsilon-\epsilon^3} - \frac{9\eta}{2R^2}\int_{-\infty}^{t} dt'\dot{v}(t') \times h_\epsilon(t-t') + \frac{3}{4\pi R^3}F(t), \tag{2}$$

where ρ_s is the density of the sphere. By comparing with the exact result[50] for the special case of the motion with constant velocity, it was argued that Eq. (2) is a reasonable approximation for $\epsilon \lesssim 0.25$[40] (see also Appendix D). The functional form of $h_\epsilon(t)$ is such that $h_0(t) = R\sqrt{\frac{\rho_f}{\pi\eta t}}$ (Appendix A) so that for $\epsilon = 0$, we obtain the familiar Basset-Boussinesq-Oseen equation[32,51–53] for an accelerating sphere in a fluid

$$\left(\rho_s + \frac{\rho_f}{2}\right)\dot{v} = -\frac{9\eta}{2R^2}v - \frac{9}{2R}\sqrt{\frac{\eta\rho_f}{\pi}}\int_{-\infty}^{t} dt'\frac{\dot{v}(t')}{\sqrt{t-t'}} + \frac{3}{4\pi R^3}F(t), \tag{3}$$

where the second term on the right hand side captures the effect of the hydrodynamic memory.[51–53]

For convenience, we may rewrite the equation for synchronous movement of two spheres in terms of dimensionless quantities, defined as

$$\theta \equiv t/\tau_B, \quad u(\theta) \equiv 6\pi\eta R v(t)/F_{\max}, \quad f(\theta) \equiv F(t)/F_{\max}, \tag{4}$$

where $F_{\max}$ is the maximum value of $F(t)$ and $\tau_B \equiv (2\rho_s + \rho_f)R^2/9\eta$ is the Brownian relaxation time.[48] Then, Eq. (2) is rewritten as

$$\frac{2\rho_s(1+3\epsilon^3)+\rho_f}{(1+3\epsilon^3)(2\rho_s+\rho_f)}\frac{du}{d\theta} = -\frac{u}{1+\frac{3}{2}\epsilon-\epsilon^3} - \int_{-\infty}^{\theta} d\theta'\frac{du}{d\theta'} \times h_\epsilon(\tau_B(\theta-\theta')) + f(\theta). \tag{5}$$

The velocity $u(\theta)$ can be obtained by numerical integration of Eq. (5), by discretizing the time θ. The integral can then be performed by a simple trapezoidal rule, which gives a reasonably accurate result when the discretization is performed with step $\Delta\theta = 0.001$, as can be checked for the case of $\epsilon = 0$ where exact solutions are available for certain special cases (see Appendix C). Once $u(\theta)$ is obtained, it is then straightforward to obtain the nondimensionalized quantities x and w corresponding to position and work, respectively, by additional integration,

$$x(\theta) \equiv \int_0^\theta u(\theta')d\theta' + x(0) \equiv \frac{6\pi\eta R}{F_{\max}\tau_B}X(t), \quad w(\theta) \equiv \int_0^\theta f(\theta')u(\theta')d\theta', \tag{6}$$

where $X(t)$ is the position of the sphere. In order to quantify a notion of efficiency for transport, we define the dimensionless effective transport drive force f_{drive},[57]

$$f_{\text{drive}} \equiv \frac{w(\theta)}{\Delta x(\theta)}, \tag{7}$$

where $\Delta x(\theta) \equiv x(\theta) - x(0)$ is the displacement. This quantity is the dimensionless version of the specific energy consumption, often used for the measure of transport efficiency in the transportation industry.[60,61] Smaller values of $f_{\text{drive}}(\theta)$ imply less external work required for a given displacement. We also define the dimensionless effective friction[57]

$$z(\theta) \equiv \frac{f_{\text{drive}}(\theta)}{\bar{u}(\theta)} = \frac{w(\theta)\Delta\theta}{\Delta x(\theta)^2}. \tag{8}$$

III. IMPROVED TRANSPORT OF TWO NEIGHBORING SPHERES

We now consider a simple protocol where a constant external force is applied over a finite duration T_{pulse}, starting from $t = 0$. Note that by definition, the maximum value of the normalized force $f(\theta)$ is unity. Therefore, $f(\theta) = 1$ for $0 \le \theta \le \theta_{\text{pulse}}$ and zero otherwise, where $\theta_{\text{pulse}} \equiv T_{\text{pulse}}/\tau_B$. We also take $x(0) = u(0) = 0$. Therefore, the input work is $w(\theta) = f \times x(\theta) = x(\theta)$ for $\theta < \theta_{\text{pulse}}$ and $w = x(\theta_{\text{pulse}})$ otherwise. As such,

$$f_{\text{drive}}(\theta) \equiv \frac{w(\theta)}{x(\theta)} = \begin{cases} 1, & (\theta < \theta_{\text{pulse}}) \\ x(\theta_{\text{pulse}})/x(\theta), & (\theta \ge \theta_{\text{pulse}}). \end{cases} \tag{9}$$

The results of the numerical computation for $\theta_{\text{pulse}} = 20$ and $\rho_s = \rho_f$ are shown in Fig. 2, where the values of $a \equiv \frac{du}{d\theta}$, u, and x are compared for $d = \infty$, $d = 8R$, and $d = 4R$. The case of $d = \infty$ corresponds to the motion of a single sphere. We find that for a *given strength* of the external force, the magnitudes of both acceleration and deceleration

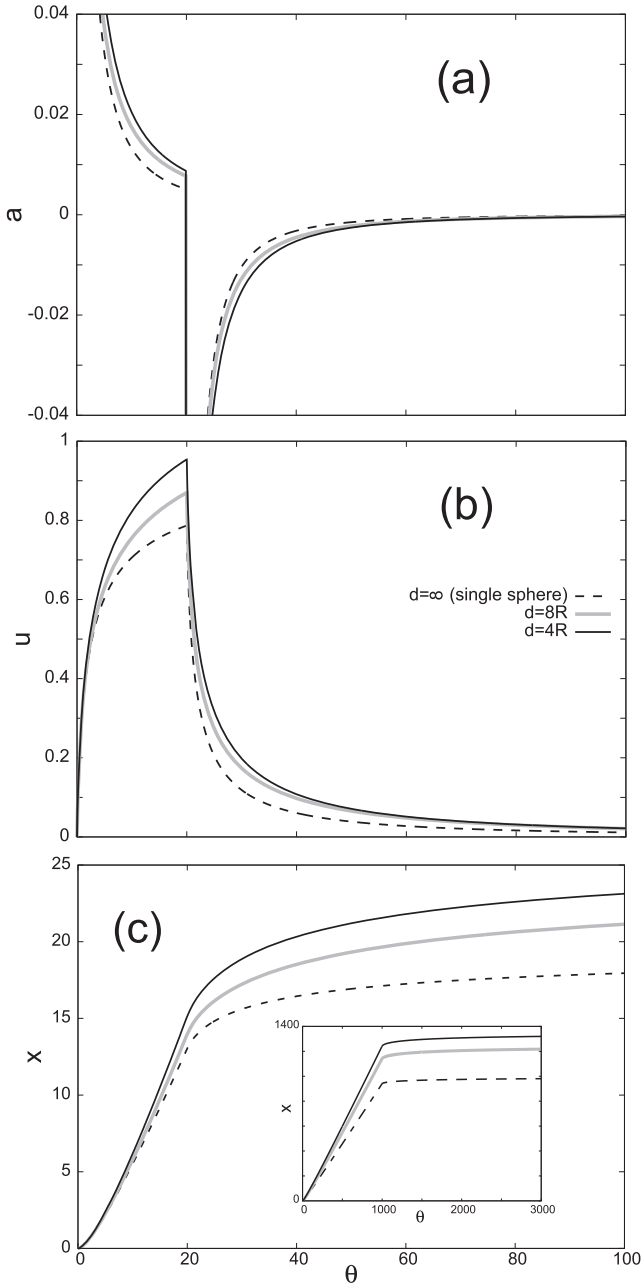

FIG. 2. (a) The nondimensional acceleration $a(\theta)$, (b) velocity $u(\theta)$, and (c) position $x(\theta)$ are compared for $d = \infty$ (single sphere), $d = 8R$, and $d = 4R$, for $T_{pulse} = 20\tau_B$ and $\rho_s = \rho_f$. The position for $T_{pulse} = 1000\tau_B$ is shown in the inset of (c).

for two neighboring spheres are larger than those for the spheres separated by a larger distance, and the overall effect is such that $v(t)$ for neighboring spheres is larger for all values of t.

More importantly, $x(\infty)$ increases by a large amount when the intersphere distance d decreases, whereas $x(\theta_{pulse})$ is only weakly dependent on distance. Therefore, from the second line of Eq. (9),

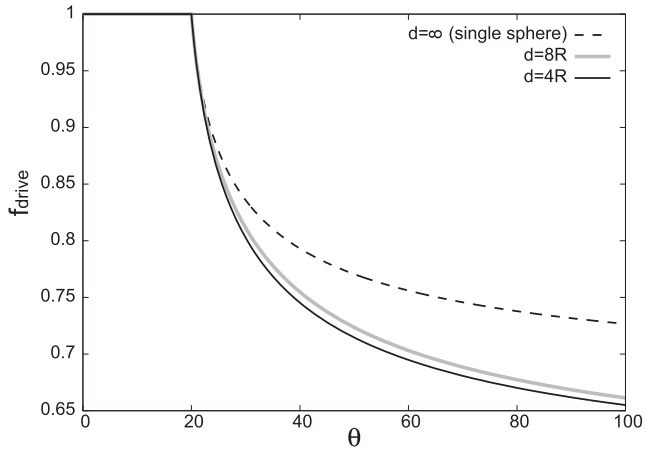

FIG. 3. The effective transport drive force $f_{drive}(\theta) \equiv w(\theta)/x(\theta)$ is compared for $d = \infty$ (single sphere), $d = 8R$, and $d = 4R$, for $T_{pulse} = 20\tau_B$ and $\rho_s = \rho_f$.

we find that $f_{drive}(\infty)$ for neighboring spheres is less than that of an isolated sphere. That is, neighboring spheres travel farther for a given amount of input work as compared to isolated spheres. The graphs of $f_{drive}(\theta)$ are shown for several values of d in Fig. 3, where we see that in fact $f_{drive}(\theta)$ is an increasing function of d for all values of θ. The values of $f_{drive}(\infty)$ are also plotted in Fig. 4 for several values of R/d and θ_{pulse}, where approximate values of $x(\infty)$ are obtained from the values of $x(\theta)$ in those approximately flat regions of the x plots (Fig. 2) with $u(\theta) \leq 0.01$. The trend of the reduced effective drive force for neighboring spheres is evident. In particular, we see that for $\theta_{pulse} = 20$, the value of f_{drive} reduces from 0.682 at $R = \infty$ to 0.596 at $d = 4R$, resulting in about ~13% reduction in the required work for a given displacement. The reduction of f_{drive} is smaller for larger values of θ_{pulse}. This is because the motion of a sphere is

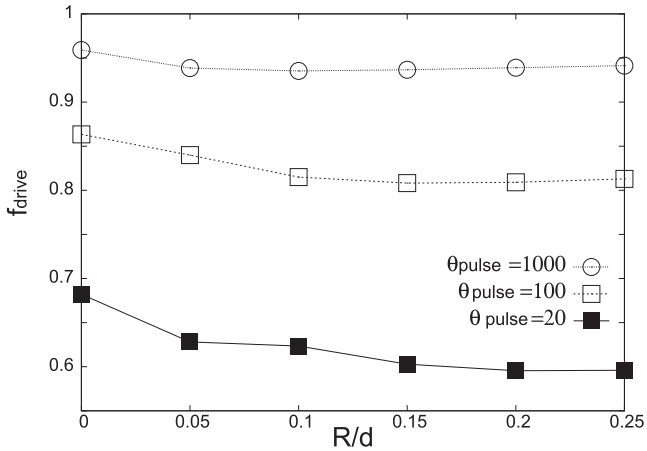

FIG. 4. The final values of the effective transport drive force, $f_{drive}(\infty) \equiv w(\infty)/x(\infty)$, are shown for several values of R/d and $\theta_{pulse} \equiv T_{pulse}/\tau_B$, with $\rho_s = \rho_f$. The case of $R/d = 0$ corresponds to that of a single sphere.

diffusive at the time scale of $t \gg \tau_B$,[32] with only tiny effects coming from hydrodynamic memory. This can be seen from the graphs of $x(\theta)$ for $\theta_{\text{pulse}} = 1000$, shown in the inset of Fig. 2(c), where the slope is approximately proportional to the instantaneous applied force, showing the typical behavior of an overdamped particle. In particular, since the motion of the sphere almost stops after the force pulse, we have $x(\theta_{\text{pulse}}) \simeq x(\infty)$, leading to $f_{\text{drive}}(\infty) = x(\theta_{\text{pulse}})/x(\infty) \simeq 1$ regardless of the intersphere distance, implying negligible reduction of the effective transport drive force.

The result also suggests that the efficiency *enhancement* is larger when the force is applied as an intermittent series of short pulses rather than one long pulse. The values of f_{drag} for two force protocols with the same average force are compared in Fig. 5. In one protocol, force is applied intermittently as ten short pulses with duration $T_{\text{pulse}} = 60\tau_B$ and magnitude $f = 2$, interspersed with the pauses of duration $T_{\text{pulse}} = 60\tau_B$. In the other protocol, a force of magnitude $f = 1$ is applied for a duration $T_{\text{pulse}} = 1200\tau_B$. The applied forces are shown at the bottom of Fig. 5 where the magnitude was rescaled by a factor of 0.5 to avoid an overlap with other curves. The resulting curves for $f_{\text{drive}}(t)$ for the intermittent short pulses and the long pulse are shown at the top and the center, respectively, where the results for $d = \infty$ (dashed) and $d = 4R$ (solid) are compared. We find that the reduction of f_{drag} due to the proximity of the other comoving sphere is greater, for the protocol of the intermittent short pulse. The reduction of f_{drag} at $t = \infty$ is 1.8% for the long pulse and 7.1% for ten short pulses. In the case of subcellular transport where a force is usually applied in a periodic manner, such as in the case of the transport due to the stepping of the kinesin motor (see Sec. IV), we expect that the movement of a neighboring object will play an important role in facilitating subcellular transport.

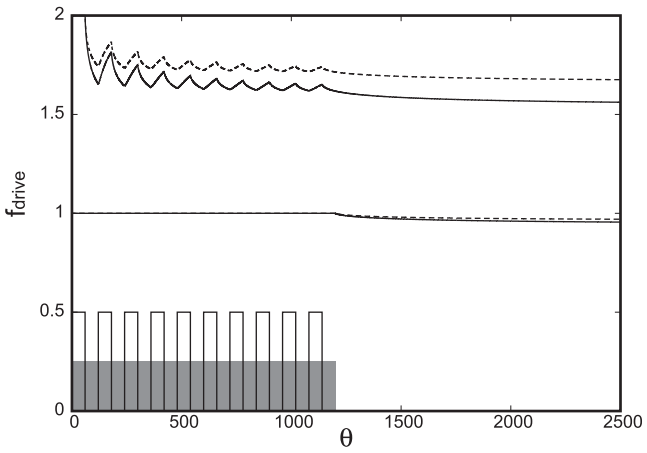

FIG. 5. The effective transport drive force is compared for two force protocols: ten short force pulses vs a constant force. The applied forces are shown at the bottom, where the intermittent and constant force protocols are shown as black lines and gray shading, respectively, and the magnitudes are scaled by 0.5 to avoid overlap with other curves. The time duration for each of the short pulses, as well as the duration of the pause, is $60\tau_B$, and the period is $120\tau_B$. The constant pulse has a time duration of $1200\tau_B$. The resulting curves for f_{drive} for the intermittent force are shown at the top for $d = \infty$ (dashed) and $d = 4R$ (solid). The results for the constant force are shown at the center for $d = \infty$ (dashed) and $d = 4R$ (solid).

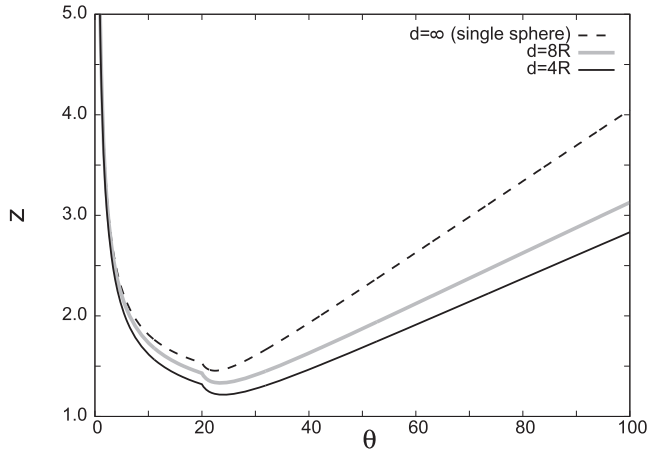

FIG. 6. The graphs of the effective transport friction $z(\theta)$ are compared for $d = \infty$ (single sphere), $d = 8R$, and $d = 4R$, for $T_{\text{pulse}} = 20\tau_B$ and $\rho_s = \rho_f$.

We also plot the graph of $z(\theta)$ in Fig. 6 for $d = \infty$ (single sphere), $d = 8R$, and $d = 4R$, showing that for given displacements, two neighboring spheres not only require less work but also result in faster transport as compared to separate spheres. The value of $z(\theta)$ here diverges as $\theta \to \infty$ because $\lim_{\theta\to\infty} \tilde{u}(\theta) = 0$, but it will be maintained at finite values when a periodic force is applied so that a nonequilibrium steady state is reached.[57]

IV. ORDER OF MAGNITUDE ESTIMATES WITH BIOLOGICAL PARAMETERS

To see whether the reduced effective transport drive force and friction due to the indirect interaction between two spheres is relevant for subcellular transport processes, we perform an order of magnitude estimate using biological parameters. More specifically, we consider an example of cargo transport by a kinesin motor, where the constant force pulse can be considered as an extremely simplified model of the force exerted by the kinesin motor and its cargo. The force duration may be taken as $T_{\text{pulse}} \sim 10\ \mu$s, the time scale during which the stepping motion occurs.[49,62–65] As discussed previously, the hydrodynamic memory plays a role only if T_{pulse} is not too much larger than $\tau_B \equiv (2\rho_s + \rho_f)R^2/9\eta$. For fixed values of T_{pulse}, ρ_s, ρ_f, and η, this tells us that the size of the cargo should be sufficiently large in order for hydrodynamic memory to play a significant role. For example, we previously found that $f_{\text{drive}}(\infty)$ for two spheres with $d = 4R$ was 13% less than for those separated by an infinite distance. Using the values $\eta = 2 \times 10^{-3}$ kg/(m s)[66–70] (BNID150903)[71] and $\rho_s = \rho_f = 10^3$ kg/m^3 (BNID113851)[72,73] for the cytoplasm, we get

$$T_{\text{pulse}} = 10\ \mu\text{s} = 20\tau_B = 20 \times \frac{3 \times 10^3\ \text{kg/m}^3 \times R^2}{9 \times 2 \times 10^{-3}\ \text{kg/(m} \cdot \text{s)}}, \tag{10}$$

leading to

$$R \simeq 2\ \mu\text{m} \sim O(1\ \mu\text{m}), \tag{11}$$

about the size of a large size vesicle such as an organelle.[74–76] Considering the fact that organelles of size of order 1 μm are often transported by molecular motors,[74–76] the reduction of effective drive force and friction driven by hydrodynamic effects warrants further investigation within living environments.

V. DISCUSSION

In this work, we presented a numerical solution for a synchronous motion of two spherical vesicles in a viscous fluid with the same force applied to each vesicle. We found that for a given displacement for each vesicle, the required work is less for two neighboring vesicles than for those separated by a larger distance, and the former is transported faster than the latter. We also found that the difference in the required work for neighboring vs isolated spheres is *more* pronounced for intermittent short pulses of applied force rather than a long pulse, making the effect particularly relevant for subcellular transport where the force are usually applied in a periodic manner, such as in the case of the transport by kinesin. In reality, the asynchrony in vesicle transport may somewhat reduce the effect proposed here. Study of such a generalized case is straightforward, albeit technically more involved.

Our results support the idea that the efficiency of subcellular transport may be improved by hydrodynamic interaction between the neighboring vesicles. Taking thermal fluctuations explicitly into account, the transport efficiency is quantified by[13,77]

$$q \equiv \frac{Q(t)\langle \delta X(t)^2 \rangle}{\langle X(t) \rangle^2}, \tag{12}$$

where $Q(t)$ is the energy consumption up to time t, $\langle X(t) \rangle$ is the average displacement, and $\langle \delta X(t)^2 \rangle$ is the transport precision. It has been shown that $q \geq 2k_BT$, a fundamental lower bound known as the thermodynamic uncertainty principle.[78–83] Within this bound, the molecular motor that performs transport with minimal energy expenditure and with highest precision is the most efficient one by definition. Since we considered the solution to a deterministic equation, the displacement we obtained is the thermally averaged displacement for a purely time-dependent external force considered in the current work. Since the input work is proportional to $Q(t)$ for a given value of thermal efficiency, and since our results tell us that $\langle X \rangle$ for two neighboring vesicles is larger than that for separate vesicles, Eq. (12) tells us that two neighboring vesicles have higher transport efficiency due to hydrodynamic interactions if $\langle \delta X(t)^2 \rangle$ are the same for both cases. Full analysis of the transport efficiency, taking into account transport precision in the presence of the thermal fluctuations, would require more sophisticated formalism such as the fluctuating hydrodynamics.[5,44–47,84–86]

ACKNOWLEDGMENTS

J.L. was supported by the National Research Foundation of Korea, funded by the Ministry of Education (Grant No. NRF-2017R1D1A1B03031344). SS and SP were supported by ARO Grant No. W911NF-17-1-0162 for "Multi-Dimensional and Dissipative Dynamical Systems: Maximum Entropy as a Principle for Modeling Dynamics and Emergent Phenomena in Complex Systems."

APPENDIX A: EXPLICIT FORM OF THE MEMORY KERNEL FOR THE TWO-SPHERE EQUATION [EQ. (1)]

The memory kernel in Eq. (1) is given by[40]

$$h_\epsilon(t) = \frac{1}{\pi}\int_0^\infty \hat{h}_\epsilon(s) e^{-st/\tau_v} ds, \tag{A1}$$

where

$$\hat{h}_\epsilon(s) = \mathrm{Im}\left[\frac{A(s)}{B_\epsilon(s)}\right] \tag{A2}$$

with

$$\begin{aligned} A(s) &= \left(1 - i\sqrt{s} - \frac{s}{9}\right)^2 \\ B_\epsilon(s) &= s^2\left(\frac{1}{9} + \frac{\epsilon^3}{3}\right) + i\left(1 + 2\epsilon^3\right)s^{3/2} - \left(1 + 5\epsilon^3\right)s \\ &\quad - 6i\sqrt{s}\epsilon^3 + 3\epsilon^3 + 3\epsilon^2 \exp\left(-i\sqrt{s}\left(1 - \epsilon^{-1}\right)\right) \\ &\quad \times \left[\frac{s^2}{90} + \frac{is^{3/2}}{6} - \frac{s}{2} - i\sqrt{s} + 1\right]\left(i\sqrt{s} - \epsilon\right) \end{aligned} \tag{A3}$$

and $\tau_v \equiv \rho_f R^2/\eta$. We note that for $\epsilon \to 0$, contribution from the term with the factor $\exp\left(-i\sqrt{s}\left(1 - \epsilon^{-1}\right)\right)$ vanishes in the integral Eq. (A1), and we have

$$\begin{aligned} h_\epsilon(t) &= \frac{1}{\pi}\int_0^\infty \mathrm{Im}\left[\frac{\left(1 - i\sqrt{s} - \frac{s}{9}\right)^2}{\frac{s^2}{9} + is^{3/2} - s}\right] e^{-st/\tau_v} ds \\ &= \frac{1}{\pi}\int_0^\infty \frac{1}{\sqrt{s}} e^{-st/\tau_v} ds = \sqrt{\frac{\tau_v}{\pi t}}, \end{aligned} \tag{A4}$$

recovering the memory kernel for one sphere.[51–53]

APPENDIX B: THE EQUATION FOR SPHERES MOVING PERPENDICULAR TO THEIR LINE OF CENTERS

In the main text, we focused on the case where the spheres move along the line connecting their centers. We may also consider two identical spheres moving perpendicular to the center-to-center axis, as shown in Fig. 7. The resulting force exerted by the fluid on each sphere is[40]

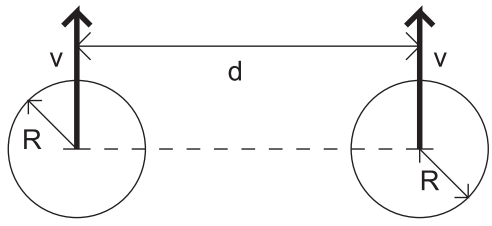

FIG. 7. Spheres moving perpendicular to the line connecting center-to-center. The directions of the velocities are shown by the bold arrows, which are also the directions of the external forces. The center-to-center distance and the radius are d and R, respectively.

$$F_{\rm fluid} = -\frac{6\pi\eta R}{1+\frac{3}{4}\epsilon+\frac{1}{2}\epsilon^3}v - \frac{2\pi R^3\rho_f}{3(1-\frac{3}{2}\epsilon^3)}\dot{v} - 6\pi\eta R\int_{-\infty}^{t} dt'\dot{v}(t')g_\epsilon(t-t'), \quad \text{(B1)}$$

where $g_\epsilon(t)$ is formally given as a Laplace transform,[40]

$$g_\epsilon(t) = \frac{1}{\pi}\int_0^\infty \hat{g}_\epsilon(s)e^{-st/\tau_v}ds, \quad \text{(B2)}$$

where

$$\hat{g}_\epsilon(s) = \mathrm{Im}\left[\frac{A(s)}{C_\epsilon(s)}\right] \quad \text{(B3)}$$

with

$$A(s) = \left(1-i\sqrt{s}-\frac{s}{9}\right)^2$$
$$C_\epsilon(s) = s^2\left(\frac{1}{9}-\frac{\epsilon^3}{6}\right)+i(1-\epsilon^3)s^{3/2}-\left(1-\frac{5}{2}\epsilon^3\right)s + 3i\sqrt{s}\epsilon^3-\frac{3}{2}\epsilon^3+\frac{3\epsilon}{2}\exp\left(-i\sqrt{s}\left(1-\epsilon^{-1}\right)\right) \times\left[\frac{s^2}{90}+\frac{is^{3/2}}{6}-\frac{s}{2}-i\sqrt{s}+1\right]\left(-s-i\sqrt{s}\epsilon+\epsilon^2\right) \quad \text{(B4)}$$

and $\tau_v \equiv \rho_f R^2/\eta$. We note that for $\epsilon \to 0$, contribution from the term with the factor $\exp\left(-i\sqrt{s}\left(1-\epsilon^{-1}\right)\right)$ vanishes in the integral Eq. (A1), and we have

$$g_\epsilon(t) = \frac{1}{\pi}\int_0^\infty \mathrm{Im}\left[\frac{(1-i\sqrt{s}-\frac{s}{9})^2}{\frac{s^2}{9}+is^{3/2}-s}\right]e^{-st/\tau_v}ds = \frac{1}{\pi}\int_0^\infty \frac{1}{\sqrt{s}}e^{-st/\tau_v}ds = \sqrt{\frac{\tau_v}{\pi t}}, \quad \text{(B5)}$$

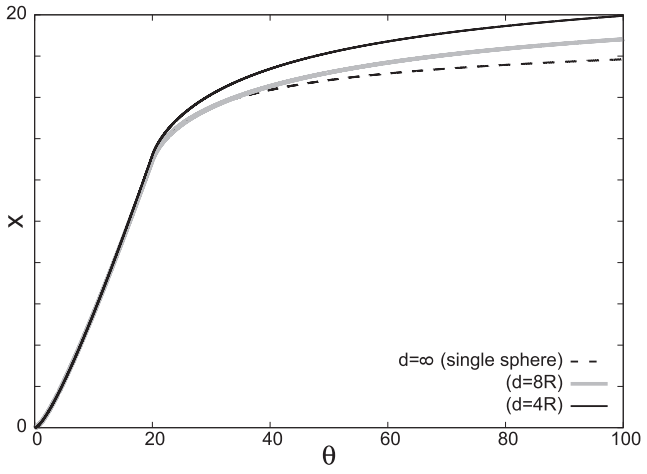

FIG. 8. The nondimensional positions $x(\theta)$ of two spheres moving perpendicular to the center-to-center line are compared for $d = \infty$ (single sphere), $d = 8R$, and $d = 4R$, for $T_{\rm pulse} = 20\tau_B$ and $\rho_s = \rho_f$.

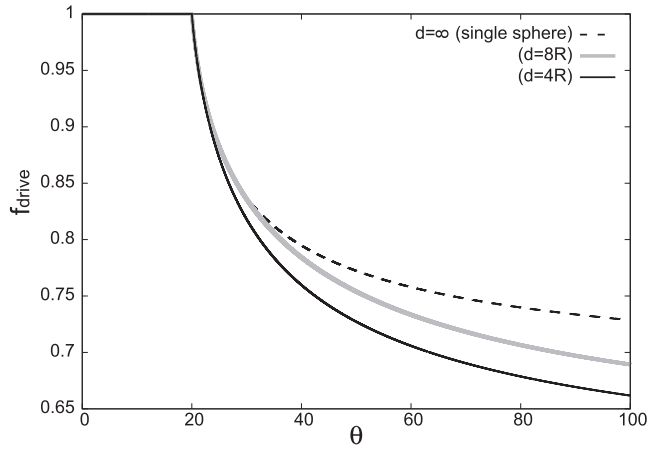

FIG. 9. The effective transport drive force $f_{\rm drive}(\theta)$ of two spheres moving perpendicular to the center-to-center line are compared for $d = \infty$ (single sphere), $d = 8R$, and $d = 4R$, for $T_{\rm pulse} = 20\tau_B$ and $\rho_s = \rho_f$.

recovering the memory kernel for one sphere.[51–53] The qualitative behavior for two neighboring spheres moving in the direction perpendicular to the central line is similar to those moving along the central line, in that the transport is enhanced, as shown in Figs. 8 and 9, where both positions and the transport drive force are compared. We again find about 13% reduction in transport drive force for $d = 4R$.

APPENDIX C: NUMERICAL SOLUTION OF THE INTEGRO-DIFFERENTIAL EQUATION

We numerically solved the integro-differential Eq. (5), rewritten as

$$a(\theta) = -F(\epsilon)G(\epsilon)u(\theta) - F(\epsilon)\int_0^\theta d\theta' a(\theta')\tilde{h}_\epsilon(\theta-\theta') + F(\epsilon)f(\theta), \quad \text{(C1)}$$

where we assumed that $v = 0$ for $\theta \le 0$, with

$$a(\theta) \equiv \frac{du}{d\theta}$$
$$\tilde{h}_\epsilon(\theta) \equiv h_\epsilon(\tau_B\theta)$$
$$F(\epsilon) \equiv \frac{(1+3\epsilon^3)(2\rho_s+\rho_f)}{2\rho_s(1+3\epsilon^3)+\rho_f} \quad \text{(C2)}$$
$$G(\epsilon) \equiv \frac{1}{1+\frac{3}{2}\epsilon-\epsilon^3}.$$

The integral in Eq. (C1) is performed by using the trapezoidal rule, where we compute an integral of the form $\int_a^b f(x)dx$ by first discretizing the interval $[a, b]$ into N subintervals and approximating the integral in each subinterval as an area of the trapezoid,

$$\int_{a+k\Delta x}^{a+(k+1)\Delta x} f(x)dx \simeq \Delta x\left[\frac{1}{2}f(a+k\Delta x)+\frac{1}{2}f(a+(k+1)\Delta x\right], \quad \text{(C3)}$$

where $\Delta x \equiv (b-a)/N$. Care must be taken when the function $f(x)$ is divergent at a boundary, say at $x = b$. Here, we cannot use Eq. (C3)

at the subinterval $[b-\Delta x, b]$, so the corresponding integral must be treated separately. We utilize the asymptotic form for the function $f(x)$ for $x \to b$,

$$f(x) \sim \frac{A}{(b-x)^{\alpha}} \quad (0 < \alpha < 1), \tag{C4}$$

to make the approximation

$$\int_{b-\Delta x}^{b} f(x)dx \simeq \int_{b-\Delta x}^{b} \frac{A}{(b-x)^{\alpha}} = \frac{A(b-\Delta x)^{1-\alpha}}{1-\alpha}. \tag{C5}$$

By using Eqs. (C3) and (C5), we obtain

$$\int_{a}^{b} f(x)dx \simeq \Delta x\left[\frac{1}{2}f(a) + \sum_{k=1}^{N-2} f(a+k\Delta x) + \frac{1}{2}f(b-\Delta x)\right] + \frac{A(b-\Delta x)^{1-\alpha}}{1-\alpha}. \tag{C6}$$

For the integral in Eq. (C1), we have

$$\int_{0}^{\theta} d\theta' a(\theta')\tilde{h}_{\epsilon}(\theta-\theta') \simeq \Delta\theta\left[\frac{1}{2}a(0)\tilde{h}_{\epsilon}(\theta) + \sum_{k=1}^{N-2} a(k\Delta\theta)\tilde{h}_{\epsilon}(\theta-k\Delta\theta) + \frac{1}{2}a(\theta-\Delta\theta)\tilde{h}_{\epsilon}(\Delta\theta)\right] + \int_{\theta-\Delta\theta}^{\theta} a(\theta')\tilde{h}_{\epsilon}(\theta-\theta')d\theta'. \tag{C7}$$

The last integral must be treated separately using Eq. (C5) since $\tilde{h}_{\epsilon}(\theta)$ diverges at $\theta = 0$. Therefore, we have to find the asymptotic form $\tilde{h}_{\epsilon}(\theta)$ for $\theta \to 0$. In fact, from Eq. (A1), we see that $h_{\epsilon}(t)$ is dominated by the value of $\hat{h}_{\epsilon}(s)$ at $s \to \infty$ as $t \to 0$. The oscillatory contribution containing the factor $e^{-i\sqrt{s}(1-\epsilon^{-1})}$ vanishes as $s \to \infty$, and we have

$$\begin{aligned}
h_{\epsilon}(t) &\simeq \frac{1}{\pi}\int_{0}^{\infty} \mathrm{Im}\left[\frac{(1-i\sqrt{s}-\frac{s}{9})^2}{s^2(\frac{1}{9}+\frac{\epsilon^3}{3}) + i(1+2\epsilon^3)s^{3/2} + O(s)}\right] e^{-st/\tau_v} ds \\
&= \frac{1}{\pi}\int_{0}^{\infty} \mathrm{Im}\left[\frac{s^2 + 18is^{3/2} + O(s)}{s^2(9+27\epsilon^3) + i81(1+2\epsilon^3)s^{3/2} + O(s)}\right] e^{-st/\tau_v} ds \\
&= \frac{1}{\pi}\int_{0}^{\infty} \mathrm{Im}\left[\frac{\left(s^2 + 18is^{3/2} + O(s)\right)\left(s^2(9+27\epsilon^3) - i81(1+2\epsilon^3)s^{3/2} + O(s)\right)}{s^4(9+27\epsilon^3)^2 + O(s^3)}\right] e^{-st/\tau_v} ds \\
&= \frac{1}{\pi}\int_{0}^{\infty} \mathrm{Im}\left[\frac{(1/9+\epsilon^3/3) + i(1+4\epsilon^3)s^{-1/2} + O(s^{-1})}{(1+3\epsilon^3)^2 + O(s^{-1/2})}\right] e^{-st/\tau_v} ds \\
&\simeq \frac{1}{\pi}\int_{0}^{\infty} \frac{1+4\epsilon^3}{(1+3\epsilon^3)^2\sqrt{s}} e^{-st/\tau_v} ds = \frac{1+4\epsilon^3}{(1+3\epsilon^3)^2}\sqrt{\frac{\tau_v}{\pi t}},
\end{aligned} \tag{C8}$$

and consequently,

$$\begin{aligned}
\int_{\theta-\Delta\theta}^{\theta} a(\theta')\tilde{h}_{\epsilon}(\theta-\theta')d\theta' &\simeq \int_{\theta-\Delta\theta}^{\theta} \frac{(1+4\epsilon^3)a(\theta')}{(1+3\epsilon^3)^2}\sqrt{\frac{\tau_v}{\pi\tau_B(\theta-\theta')}}d\theta' \\
&\simeq a(\theta)\int_{\theta-\Delta\theta}^{\theta} \frac{(1+4\epsilon^3)}{(1+3\epsilon^3)^2}\sqrt{\frac{\tau_v}{\pi\tau_B(\theta-\theta')}}d\theta' \\
&= \frac{2(1+4\epsilon^3)}{(1+3\epsilon^3)^2}\sqrt{\frac{\tau_v\Delta\theta}{\pi\tau_B}}a(\theta).
\end{aligned} \tag{C9}$$

Note that the right-hand side of Eq. (C1) contains $u(\theta)$ that is undetermined at the time when computing $a(\theta)$. It is to be computed using the trapezoidal rule

$$u(\theta) = u(\theta-\Delta\theta) + \frac{\Delta\theta}{2}[a(\theta) + a(\theta-\Delta\theta)]. \tag{C10}$$

We simply substitute Eq. (C10) into Eq. (C1), along with and Eqs. (C7) and (C9) to get

$$\begin{aligned}
a(\theta) = &-F(\epsilon)G(\epsilon)u(\theta-\Delta\theta) - \frac{\Delta\theta}{2}F(\epsilon)G(\epsilon)[a(\theta)+a(\theta-\Delta\theta)] \\
&-F(\epsilon)\Delta\theta\left[\frac{1}{2}a(0)\tilde{h}_{\epsilon}(\theta) + \sum_{k=1}^{N-2} a(k\Delta\theta)\tilde{h}_{\epsilon}(\theta-k\Delta\theta)\right. \\
&\left. + \frac{1}{2}a(\theta-\Delta\theta)\tilde{h}_{\epsilon}(\Delta\theta)\right] - F(\epsilon)\frac{2(1+4\epsilon^3)}{(1+3\epsilon^3)^2} \\
&\times\sqrt{\frac{\tau_v\Delta\theta}{\pi\tau_B}}a(\theta) + F(\epsilon)f(\theta).
\end{aligned} \tag{C11}$$

After moving the term proportional to $a(\theta)$ and solving for $a(\theta)$, Eq. (C11)

$$\begin{aligned}
a(\theta) = &-H(\epsilon)F(\epsilon)G(\epsilon)u(\theta-\Delta\theta) \\
&-H(\epsilon)F(\epsilon)\Delta\theta\left[\frac{1}{2}a(0)\tilde{h}_{\epsilon}(\theta) + \sum_{k=1}^{N-2} a(k\Delta\theta)\tilde{h}_{\epsilon}(\theta-k\Delta\theta)\right. \\
&\left. + \frac{1}{2}a(\theta-\Delta\theta)\left(\tilde{h}_{\epsilon}(\Delta\theta) + G(\epsilon)\right)\right] + H(\epsilon)F(\epsilon)f(\theta),
\end{aligned} \tag{C12}$$

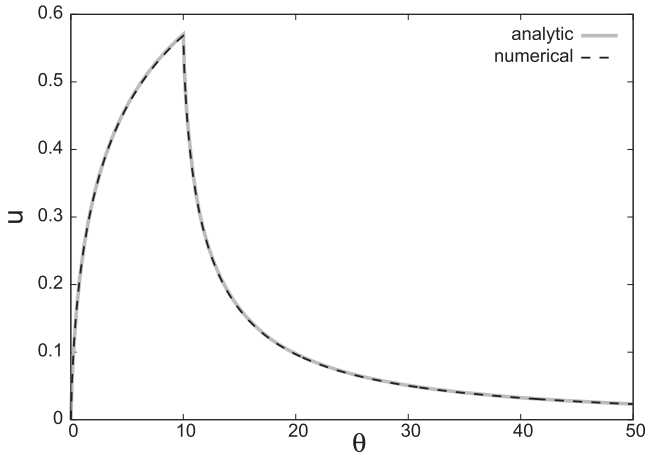

FIG. 10. The velocity of a single sphere as the function of time. Analytic and numerical solutions are compared for $\rho_s = 0$. The integration parameters are $\Delta\theta = 10^{-3}$, $\Delta s = 10^{-4}$, and $\delta = 10^{-4}$.

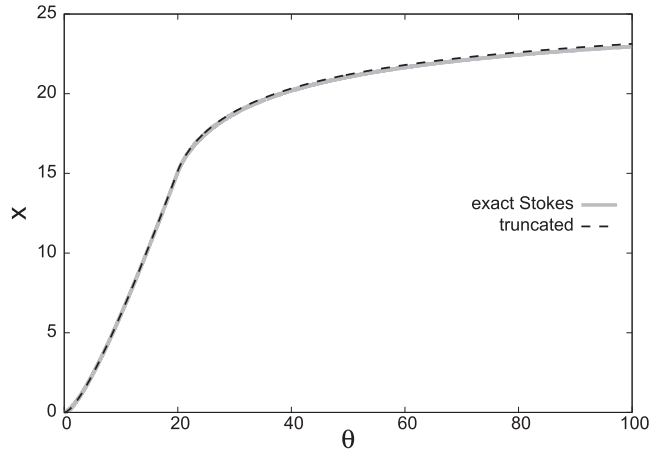

FIG. 11. The position of each sphere as the function of time. The result obtained from the truncated expression and the exact one for the Stokes drag are compared, for $t = 20\tau_B$ and $\rho_s = \rho_f$.

where

$$H(\epsilon) \equiv \left[1 + F(\epsilon)\frac{2(1+4\epsilon^3)}{(1+3\epsilon^3)^2}\sqrt{\frac{\tau_v \Delta\theta}{\pi\tau_B}} + \frac{\Delta\theta}{2}F(\epsilon)G(\epsilon)\right]^{-1}. \quad \text{(C13)}$$

Equation (C12) allows us to compute $a(\theta)$ in terms of $u(\theta - \Delta\theta)$ and $a(0)$, $a(\Delta\theta)$, ..., $a(\theta - \Delta\theta)$, by storing $a(\theta)$'s as arrays during the computation. Once $a(\theta)$ is obtained, $u(\theta)$ can be obtained by Eq. (C10).

We also need to compute the integral in Eq. (A1) in order to obtain $\tilde{h}_\epsilon(\theta)$. The upper limit of the integral is infinity, so we truncate the integral when the integrand is sufficiently small. In other words, we truncate the region with $e^{-s\tau_B\theta/\tau_v} < \delta$. The remaining integral is obtained numerically by the trapezoidal rule. It would be computationally inefficient to perform the integral in Eq. (A1) each time we compute $a(\theta)$. Therefore, we compute $\tilde{h}_\epsilon(0), \tilde{h}_\epsilon(\Delta\theta), \cdots \tilde{h}_\epsilon(N\Delta\theta)$ at the start of the computation and store them as arrays, where $N\Delta\theta$ is the upper limit of θ that $a(\theta)$ will be computed.

For an isolated sphere, an analytic solution of Eq. (3) for a constant pull is known[39] which can be compared with our numerical solution for $\epsilon = 0$ to assess the accuracy of our method. We found that using $\Delta\theta = 0.001$, $\Delta s = 0.0001$, and $\delta = 0.0001$ yields reasonably accurate solution, as can be seen in Fig. 10 where the numerical and the analytic solutions for the velocities are compared for $\rho_s = 0$.[87] These parameters were also used for performing the numerical integration of the two-sphere equation.

APPENDIX D: ASSESSMENT OF THE ACCURACY OF THE TRUNCATION IN TWO-SPHERE EQUATION

As mentioned in the main text, Eq. (5), with $h_\epsilon(t)$ given by Eqs. (A1)–(A3), is obtained by a truncation where the error is considered to be of order $O(\epsilon^4)$ where $\epsilon \equiv R/d$. It was argued in Ref. 40 that Eq. (5) is reasonably accurate for $\epsilon \lesssim 0.25$, by comparing the Stokes drag in Eq. (5),

$$f_{\text{Stokes}}^{(\text{trunc})} = -\frac{u}{1 + \frac{3}{2}\epsilon - \epsilon^3}, \quad \text{(D1)}$$

with the known exact form[50,88]

$$f_{\text{Stokes}}^{(\text{exact})} = -\frac{4u}{3}\sum_{n=1}^{\infty}\sinh\alpha\frac{n(n+1)}{(2n-1)(2n+3)} \times\left[1 - \frac{4\sinh^2(n+\frac{1}{2})\alpha - (2n+1)^2\sinh^2\alpha}{2\sinh(2n+1)\alpha + (2n+1)\sinh 2\alpha}\right], \quad \text{(D2)}$$

where

$$2\cosh\alpha \equiv \epsilon^{-1}. \quad \text{(D3)}$$

The numerical result is quite robust as we replace $f_{\text{Stokes}}^{(\text{trunc})}$ by $f_{\text{Stokes}}^{(\text{exact})}$ up to $\epsilon = 0.25$, as shown in Fig. 11 where the results for the position x are compared for $t = 20\tau_B$ and $\rho_s = \rho_f$. This provides circumstantial evidence that Eq. (5), along with Eqs. (A1)–(A3), is quite accurate for $\epsilon \lesssim 0.25$. We however do not use $f_{\text{Stokes}}^{\text{exact}}$ as we avoid *ad hoc* mixing of exact and truncated expressions.

REFERENCES

[1] P. Pietzonka, A. C. Barato, and U. Seifert, "Universal bound on the efficiency of molecular motors," J. Stat. Mech.: Theory Exp. **2016**, 124004.
[2] K. Kinosita, Jr., R. Yasuda, H. Noji, and K. Adachi, "A rotary molecular motor that can work at near 100% efficiency," Philos. Trans. R. Soc., B **355**, 473 (2000).
[3] H. Wang and G. Oster, "The Stokes efficiency for molecular motors and its applications," Europhys. Lett. **57**, 134 (2002).
[4] T. Schmiedl and U. Seifert, "Efficiency of molecular motors at maximum power," Europhys. Lett. **83**, 30005 (2008).
[5] M. S. Liu, B. D. Todd, and R. J. Sadus, "Kinetics and chemomechanical properties of the F1-ATPase molecular motor," J. Chem. Phys. **118**, 9890 (2003).
[6] A. W. Lau, D. Lacoste, and K. Mallick, "Nonequilibrium fluctuations and mechanochemical couplings of a molecular motor," Phys. Rev. Lett. **99**, 158102 (2007).
[7] T. Ariga, M. Tomishige, and D. Mizuno, "Nonequilibrium energetics of molecular motor kinesin," Phys. Rev. Lett. **121**, 218101 (2018).

[8]A. B. Kolomeisky, "Motor proteins and molecular motors: How to operate machines at the nanoscale," J. Phys.: Condens. Matter **25**, 463101 (2013).
[9]A. B. Kolomeisky and M. E. Fisher, "Molecular motors: A theorist's perspective," Annu. Rev. Phys. Chem. **58**, 675–695 (2007).
[10]W. Hwang and C. Hyeon, "Quantifying the heat dissipation from molecular motor's transport properties in nonequilibrium steady states," J. Phys. Chem. Lett. **8**, 250–256 (2017).
[11]C. Bustamante, D. Keller, and G. Oster, "The physics of molecular motors," Acc. Chem. Res. **34**, 412–420 (2001).
[12]A. I. Brown and D. A. Sivak, "Allocating dissipation across a molecular machine cycle to maximize flux," Proc. Natl. Acad. Sci. U. S. A. **114**, 11057–11062 (2017).
[13]W. Hwang and C. Hyeon, "Energetic costs, precision, and transport efficiency of molecular motors," J. Phys. Chem. Lett. **9**, 513–520 (2018).
[14]R. M. Jendrejack, M. D. Graham, and J. J. de Pablo, "Hydrodynamic interactions in long chain polymers: Application of the Chebyshev polynomial approximation in stochastic simulations," J. Chem. Phys. **113**, 2894 (2000).
[15]R. M. Jendrejack, J. J. de Pablo, and M. D. Graham, "Stochastic simulations of DNA in flow: Dynamics and the effects of hydrodynamic interactions," J. Chem. Phys. **116**, 7752 (2002).
[16]B. Liu and B. Dünweg, "Translational diffusion of polymer chains with excluded volume and hydrodynamic interactions by Brownian dynamics simulation," J. Chem. Phys. **118**, 8061 (2003).
[17]T. Geyera and U. Winter, "An O(N^2) approximation for hydrodynamic interactions in Brownian dynamics simulations," J. Chem. Phys. **130**, 114905 (2009).
[18]A. Donev and E. Vanden-Eijnden, "Dynamic density functional theory with hydrodynamic interactions and fluctuations," J. Chem. Phys. **140**, 234115 (2014).
[19]M. Kröger, A. Alba-Pérez, M. Laso, and H. C. Öttinger, "Variance reduced Brownian simulation of a bead-spring chain under steady shear flow considering hydrodynamic interaction effects," J. Chem. Phys. **113**, 4767 (2000).
[20]W. Jiang, J. Huang, Y. Wang, and M. Laradji, "Hydrodynamic interaction in polymer solutions simulated with dissipative particle dynamics," J. Chem. Phys. **126**, 044901 (2007).
[21]T. Eckert and W. Richtering, "Thermodynamic and hydrodynamic interaction in concentrated microgel suspensions: Hard or soft sphere behavior?," J. Chem. Phys. **129**, 124902 (2008).
[22]N. Hoda and S. Kumar, "Brownian dynamics simulations of polyelectrolyte adsorption in shear flow with hydrodynamic interaction," J. Chem. Phys. **127**, 234902 (2007).
[23]U. S. Agarwal, "Effect of initial conformation, flow strength, and hydrodynamic interaction on polymer molecules in extensional flows," J. Chem. Phys. **113**, 3397 (2000).
[24]V. Lisy, J. Tothova, and A. V. Zatovsky, "Comparison of Brownian dynamics algorithms with hydrodynamic interaction," J. Chem. Phys. **135**, 084116 (2011).
[25]A. Daddi-Moussa-Idera and S. Gekle, "Hydrodynamic interaction between particles near elastic interfaces," J. Chem. Phys. **145**, 014905 (2016).
[26]S. Henderson, S. Mitchell, and P. Bartlett, "Propagation of hydrodynamic interactions in colloidal suspensions," Phys. Rev. Lett. **88**, 088302 (2002).
[27]T. B. Liverpool and F. C. MacKintosh, "Inertial effects in the response of viscous and viscoelastic fluids," Phys. Rev. Lett. **95**, 208303 (2005).
[28]M. Atakhorrami, G. H. Koenderink, C. F. Schmidt, and F. C. MacKintosh, "Short-time inertial response of viscoelastic fluids: Observation of vortex propagation," Phys. Rev. Lett. **95**, 208302 (2005).
[29]V. Lisy, J. Tothova, and A. V. Zatovsky, "Long-time dynamics of Rouse-Zimm polymers in dilute solutions with hydrodynamic memory," J. Chem. Phys. **121**, 10699 (2004).
[30]R. Huang, I. Chavez, K. M. Taute, B. Lukić, S. Jeney, M. G. Raizen, and E.-L. Florin, "Direct observation of the full transition from ballistic to diffusive Brownian motion in a liquid," Nat. Phys. **7**, 576–580 (2011).
[31]T. Franosch, M. Grimm, M. Belushkin, F. M. Mor, G. Foffi, L. Forró, and S. Jeney, "Resonances arising from hydrodynamic memory in Brownian motion," Nature **478**, 85–88 (2011).
[32]S. Kheifets, A. Simha, K. Melin, T. Li, and M. G. Raizen, "Observation of Brownian motion in liquids at short times: Instantaneous velocity and memory loss," Science **343**, 1493–1496 (2014).
[33]B. J. Alder and T. E. Wainwright, "Decay of the velocity autocorrelation function," Phys. Rev. A **1**, 18–20 (1970).
[34]Y. W. Kim and J. E. Matta, "Long-time behavior of the velocity autocorrelation: A measurement," Phys. Rev. Lett. **31**, 208–210 (1973).
[35]P. D. Fedele and Y. W. Kim, "Direct measurement of the velocity autocorrelation function for a Brownian test particle," Phys. Rev. Lett. **44**, 691 (1980).
[36]M. Parmar, A. Haselbacher, and S. Balachandar, "Generalized Basset-Boussinesq-Oseen equation for unsteady forces on a sphere in a compressible flow," Phys. Rev. Lett. **106**, 084501 (2011).
[37]D. Lesnicki and R. Vuilleumier, "Molecular hydrodynamics from memory kernels," Phys. Rev. Lett. **116**, 147804 (2016).
[38]G. Jung and F. Schmid, "Frequency-dependent hydrodynamics interaction between two solid spheres," Phys. Fluids **29**, 126101 (2017).
[39]L. Arminski and S. Weinbaum, "Effect of waveform and duration of impulse on the solution to the Basset-Langevin equation," Phys. Fluids **22**, 404–411 (1979).
[40]A. M. Ardekani and R. H. Rangel, "Unsteady motion of two solid spheres in Stokes flow," Phys. Fluids **18**, 103306 (2006).
[41]B. U. Felderhof, "Retarded hydrodynamic interaction between two spheres immersed in a viscous incompressible fluid," Phys. Fluids **31**, 053604 (2019).
[42]M. C. Marchetti, J. F. Joanny, S. Ramaswamy, T. B. Liverpool, J. Prost, M. Rao, and R. A. Simha, "Hydrodynamics of soft active matter," Rev. Mod. Phys. **85**, 1143 (2013).
[43]G. Salbreux, J. Prost, and J. F. Joanny, "Hydrodynamics of cellular cortical flows and the formation of contractile rings," Phys. Rev. Lett. **103**, 058102 (2009).
[44]J. T. Padding and A. A. Louis, "Hydrodynamic and Brownian fluctuations in sedimenting suspensions," Phys. Rev. Lett. **93**, 220601 (2004).
[45]W. Wu, F. Zhang, and J. Wang, "Potential landscape and flux field theory for turbulence and nonequilibrium fluid systems," Ann. Phys. **389**, 63–101 (2018).
[46]C. Cattuto, R. Brito, U. M. B. Marconi, F. Nori, and R. Soto, "Fluctuation-induced Casimir forces in granular fluids," Phys. Rev. Lett. **96**, 178001 (2006).
[47]F. Detcheverry and L. Bocquet, "Thermal fluctuations in nanofluidic transport," Phys. Rev. Lett. **109**, 024501 (2012).
[48]J. T. Padding and A. A. Louis, "Hydrodynamic interactions and Brownian forces in colloidal suspensions: Coarse-graining over time and length scales," Phys. Rev. E **74**, 031402 (2006).
[49]Y. Goldtzvik, Z. Zhang, and D. Thirumalai, "Importance of hydrodynamic interactions in the stepping kinetics of kinesin," J. Phys. Chem. B **120**, 2071–2075 (2016).
[50]M. Stimson and G. Jeffery, "The motion of two spheres in a viscous fluid," Proc. R. Soc. London, Ser. A **111**, 110 (1926).
[51]J. Boussinesq, "Sur la resistance qu'oppose un liquide indefini en repos, sans pesanteur, au mouvement varie d'une sphere solide qu'il mouille sur toute sa surface, quand les vitesses restent bien continues et assez faibles pour que leurs carres et produits soient negligiables," C. R. Acad. Sci. Paris **100**, 935 (1885).
[52]A. Basset, Philos. Trans. R. Soc., A **179**, 43 (1888).
[53]C. Oseen, *Hydrodynamik* (Akademische Verlagsgesellschaft, Leipzig, 1927).
[54]H. J. H. Clercx and P. P. J. M. Schram, "Brownian particles in shear flow and harmonic potentials: A study of long-time tails," Phys. Rev. A **46**, 1942–1950 (1992).
[55]M. van Aartrijk and H. J. H. Clercx, "Vertical dispersion of light inertial particles in stably stratified turbulence: The influence of the basset force," Phys. Fluids **22**, 013301 (2010).
[56]M. A. T. van Hinsberg, J. H. M. ten Thije Boonkkamp, and H. J. H. Clercx, "An efficient, second order method for the approximation of the Basset history force," J. Comput. Phys. **230**, 1465–1478 (2011).
[57]S. L. Seyler and S. Pressé, "Long-time persistence of hydrodynamic memory boosts microparticle transport," e-print arXiv:1906.04957 (2019).
[58]Reference 41 appeared after we completed the manuscript. Both the equations in Refs. 40 and 41 describe the unsteady motion of two hard spheres in incompressible viscous fluid and use approximations that are valid only when the distance between the two spheres is sufficiently large. The improvements in Ref. 41 are

twofold. First, it includes the rotation of each sphere, which is irrelevant for our result where the rotations are not considered. Second, a better approximation is used so that the equation is valid up to shorter distances compared to that in Ref. 40. We checked that for the intersphere distances considered in this work, the results generated by the equation in Ref. 41 result in no visible changes to the figures we present in the manuscript.

[59]L. D. Landau and E. M. Lifshitz, *Fluid Mechanics* (Pergamon Press, Oxford, 1987).

[60]M. Trancossi, "What price of speed? A critical revision through constructional optimization of transport modes," Int. J. Energy Environ. Eng. **7**, 425 (2016).

[61]B. D. Chiara, D. D. Franco, N. Coviello, and D. Pastrone, "Comparative specific energy consumption between air transport and high-speed rail transport: A practical assessment," Transp. Res. Part D: Transp. Environ. **52**, 227 (2017).

[62]N. J. Carter and R. A. Cross, "Mechanics of the kinesin step," Nature **435**, 308–312 (2005).

[63]Z. Zhang and D. Thirumalai, "Dissecting the kinematics of the kinesin step," Structure **20**, 628–640 (2012).

[64]J. Kubelka, J. Hofrichter, and W. A. Eaton, "The protein folding 'speed limit,'" Curr. Opin. Struct. Biol. **14**, 76–88 (2004).

[65]This time scale is shorter than folding time for some small single-domain proteins,[64] although the kinesin stepping involves the rearrangement of a larger polypeptide segment. This ultrafast behavior may be due to the fact that the kinesin stepping is an active process involving ATP hydrolysis.

[66]T. Ando and J. Skolnick, "Crowding and hydrodynamic interactions likely dominate *in vivo* macromolecular motion," Proc. Natl. Acad. Sci. U. S. A. **107**, 18457–18462 (2010).

[67]K. Luby-Phelps, "Cytoarchitecture and physical properties of cytoplasm: Volume, viscosity, diffusion, intracellular surface area," in *International Review of Cytology* (Academic Press, 1999), Vol. 192, pp. 189–221.

[68]D. Ridgway, G. Broderick, A. Lopez-Campistrous, M. Ru'aini, P. Winter, M. Hamilton, P. Boulanger, A. Kovalenko, and M. J. Ellison, "Coarse-grained molecular simulation of diffusion and reaction kinetics in a crowded virtual cytoplasm," Biophys. J. **94**, 3748–3759 (2008).

[69]A. S. Verkma, "Solute and macromolecule diffusion in cellular aqueous compartments," Trends Biochem. Sci. **27**, 27–33 (2002).

[70]R. Milo, P. Jorgensen, U. Moran, G. Weber, and M. Springer, "Bionumbers—The database of key numbers in molecular and cell biology," Nucleic Acids Res. **38**, D750–D753 (2010).

[71]The ID number of BioNumbers Database.[70]

[72]S. Heyden and M. Ortiz, "Investigation of the influence of viscoelasticity on oncotripsy," Comput. Methods Appl. Mech. Eng. **314**, 314–322 (2017).

[73]U. Moran, R. Phillips, and R. Milo, "Snapshot: Key numbers in biology," Cell **141**, 1–2 (2010).

[74]H. Lodish, A. Berk, S. L. Zipursky, P. Matsudaira, D. Baltimore, and J. Darnell, *Molecular Cell Biology*, 4th ed. (W. H. Freeman, New York, 2000).

[75]N. Hirokawa, "Kinesin and dynein superfamily proteins and the mechanism of organelle transport," Science **279**, 519–526 (1998).

[76]W. O. Hancock, "Bidirectional cargo transport: Moving beyond tug-of-war," Nat. Rev. Mol. Cell Biol. **15**, 615–628 (2014).

[77]A. Dechant and S.-I. Sasa, "Current fluctuations and transport efficiency for general Langevin systemsocating dissipation across a molecular machine cycle to maximize flux," J. Stat. Mech.: Theory Exp. **2018**, 063209.

[78]A. C. Barato and U. Seifert, "Thermodynamic uncertainty relation for biomolecular processes," Phys. Rev. Lett. **114**, 158101 (2015).

[79]T. R. Gingrich, J. M. Horowitz, N. Perunov, and J. L. England, "Dissipation bounds all steady-state current fluctuations," Phys. Rev. Lett. **116**, 120601 (2016).

[80]P. Pietzonka, A. C. Barato, and U. Seifert, "Universal bounds on current fluctuations," Phys. Rev. E **93**, 052145 (2016).

[81]S. Pigolotti, I. Neri, E. Roldán, and F. Jülicher, "Generic properties of stochastic entropy production," Phys. Rev. Lett. **119**, 140604 (2017).

[82]C. Hyeon and W. Hwang, "Physical insight into the thermodynamic uncertainty relation using Brownian motion in tilted periodic potentials," Phys. Rev. E **96**, 012156 (2017).

[83]K. Proesmans and C. Van den Broeck, "Discrete-time thermodynamic-like uncertainty relation," Europhys. Lett. **119**, 20001 (2017).

[84]N. K. Voulgarakis and J.-W. Chu, "Bridging fluctuating hydrodynamics and molecular dynamics simulations of fluids," J. Chem. Phys. **130**, 134111 (2009).

[85]G. Giupponi, G. D. Fabritiis, and P. V. Coveney, "Hybrid method coupling fluctuating hydrodynamics and molecular dynamics for the simulation of macromolecules," J. Chem. Phys. **126**, 154903 (2007).

[86]B. Z. Shang, N. K. Voulgarakis, and J.-W. Chua, "Fluctuating hydrodynamics for multiscale simulation of inhomogeneous fluids: Mapping all-atom molecular dynamics to capillary waves," J. Chem. Phys. **135**, 044111 (2011).

[87]The analytic solution for $\rho_s = \rho_f$ is expressed in terms of error function with a complex argument.[39] For convenience, we therefore use $\rho_s = 0$ for the purpose of plotting the analytic solution.

[88]There is an error in the overall prefactor of the final expression in Ref. 50 where 2/3 is given instead of 4/3. We could check that 4/3 is the correct one by carefully following their derivation.